Research Article

Implications of submonthly oxygen and carbon isotope variations in late Pleistocene *Melanopsis* shells for regional and local hydroclimate in the upper Jordan River valley

Addison Rice[a,b]* 🔾, Elizabeth Bunin[b], Birgit Plessen[c], Gonen Sharon[d] and Steffen Mischke[b]

[a]Department of Earth Sciences, Faculty of Geosciences, Utrecht University, Princetonlaan 8a, 3584 CS Utrecht, Netherlands; [b]Institute of Earth Sciences, University of Iceland, Sturlugata 7 Askja, 102 Reykjavík, Iceland; [c]Climate Dynamics and Landscape Evolution Section, GFZ German Research Centre for Geosciences, 14473 Potsdam, Germany and [d]MA Program in Galilee Studies, East Campus, Tel-Hai College, Upper Galilee, 12208, Israel

Abstract

Many water-stressed regions of the globe have a highly seasonal precipitation regime. However, seasonality in the past and under changing climates is little studied. Submonthly records of sclerochronological $\delta^{18}O$ and $\delta^{13}C$ values of *Melanopsis* shells from the Jordan River Dureijat archaeological site (JRD) in the upper Jordan River valley presented here document the hydrology of paleo-Lake Hula. These records were assessed for changes in seasonal hydrology in the lake and compared with modern shells collected from present-day water-bodies in northern Israel and with models of $\delta^{18}O_{shell}$. Results from shells in sediments dating from the last glacial maximum (LGM) to the Bølling-Allerød imply changes in waterbody size that qualitatively parallel changes in the late Pleistocene Lake Lisan levels; Hula Lake was well buffered when Lake Lisan stood at a high stand and poorly buffered when water levels were lower. Furthermore, data from shells dated to the LGM suggest inflowing water with lower $\delta^{18}O$ values than local rainfall, providing evidence for a greater proportion of snow in the catchment than today. Reconstruction of water $\delta^{18}O$ and mixing-model calculations suggest that snowmelt contribution to spring water during the LGM may have been more than twice the amount in the modern-day catchment.

Keywords: Seasonality, Sclerochronology, Last glacial maximum, Epipaleolithic, Levant, Hula Basin

(Received 3 June 2022; accepted 11 May 2023)

INTRODUCTION

With changes in hydrology imminent as a result of anthropogenic climate change, improved knowledge of past changes in precipitation and freshwater systems is necessary to enhance the accuracy of climate models and better understand the effects of a changing climate on human society. In the Levant, or eastern Mediterranean region, large gradients in climate on small spatial scales in conjunction with predominantly seasonal precipitation generate greater uncertainties in predictions of water availability (Rambeau, 2010). Furthermore, the region's long history of human habitation makes it uniquely suited to studies on the effects of a changing climate on human society (Frumkin et al., 2011; Enzel and Bar-Yosef, 2017). However, few existing paleoclimate records can be correlated with human activity at archaeological sites (Rambeau, 2010; Enzel and Bar-Yosef, 2017). In addition, very few studies of pre-Holocene paleoseasonality have been performed in this region (Ben Dor et al., 2018, 2021;

Langgut et al., 2021; Müller et al., 2022). During the final Pleistocene, archeologically known as the Epipaleolithic (EP; 25–11.7 ka), human communities in the Levant shifted from small bands of nomadic hunter-gatherers into the earliest sedentary settlements (Belfer-Cohen and Goring-Morris, 2020). An understanding of weather patterns during this time, when human impact on the environment was minimal, may improve present climate models and enhance insight into ecological and cultural changes during the final Pleistocene (Rambeau, 2010).

Late Pleistocene paleoclimate in the Levant is largely correlated with glacial fluctuations in the Northern Hemisphere, but while some paleoclimate archives in the Levant, including pollen, lake levels, and speleothems, indicate cold and dry conditions during Heinrich events and warm, wet conditions during the Bølling-Allerød, interpretations of records dated to the last glacial maximum (LGM) are contradictory (Rossignol-Strick, 1995; Bar-Matthews et al., 1999, 2003; Bartov et al., 2002; Robinson et al., 2006; Roberts et al., 2008; Develle et al., 2011; Orland et al., 2012; Torfstein et al., 2013; Miebach et al., 2017; Matthews et al., 2021). In the LGM, levels of Lake Lisan, the precursor to the Dead Sea that stretched northward to the modern Sea of Galilee, were at a very high stand. However, the conditions that led to these high lake levels are not well understood (Bartov

et al., 2002; Hazan et al., 2005; Torfstein et al., 2013; Lev et al., 2019). For example, pollen records indicate a prevalence of steppe vegetation in the region, possibly indicating low water availability (Miebach et al., 2017, 2019; Langgut et al., 2021). Meanwhile, speleothem isotope records from caves in the Levant indicate increasing aridity, but speleothems grew in the Negev Desert, where conditions today are too arid for their formation (Bar-Matthews et al., 1999, 2003; Vaks et al., 2006). Enzel et al. (2008) suggest that storm path trajectories of the Cyprus Lows were located farther to the south during the LGM than currently, accounting for more moisture in the southern Levant. Oxygen isotope records from speleothems in the region support this hypothesis, with lower $\delta^{18}O_{speleothem}$ values to the south and north compared with central Israel during the LGM, which may indicate low $\delta^{18}O_{precipitation}$ values due to Rayleigh distillation processes outside the main storm path (Vaks et al., 2006; Bar-Matthews et al., 2019). Evidence of flooding events in Lake Lisan during the LGM support more frequent southerly storm paths (Ben Dor et al., 2018). Pollen records in the region could also support this inference; models based on pollen records suggest a similar or lower amount of precipitation than today combined with a lower temperature and lower evaporation due to decreased insolation (Miebach et al., 2019; Langgut et al., 2021). Climate modeling efforts also suggest that lower temperatures in combination with lower precipitation and evaporation played a role in the LGM climate of the Levant (Stockhecke et al., 2016; Ludwig and Hochman, 2022). Another working hypothesis is that expanded snow cover and frozen ground would result in annual melt with less contribution to soil moisture (Develle et al., 2011). The lack of speleothem growth on Mt. Hermon during the LGM implies a wider area of freezing temperatures (Ayalon et al., 2013), and dry intervals in a lake record from Yammoûneh, Lebanon, indicate an increase in storage of water as snow and/or frozen ground conditions (Develle et al., 2011), supported by evidence of glaciers in the Mt. Lebanon area during this interval (Moulin et al., 2022). Zaarur et al. (2016) reconstructed low $\delta^{18}O_{water}$ values from carbonate clumped isotopes in gastropod shells in the upper Jordan River valley, while speleothems in the more southerly Soreq Cave exhibited higher $\delta^{18}O_{speleothem}$ values during the LGM (Bar-Matthews et al., 2003). Zaarur et al. (2016) interpret their reconstructed LGM $\delta^{18}O_{water}$ values as being influenced by snowmelt from the surrounding mountains.

High-resolution (subseasonal) records such as those produced from sclerochronologically subsampled organismal remains can help to disentangle moisture sources (Taft et al., 2020; Wiese et al., 2020) and provide a seasonal perspective on geologic-scale climate change (Taft et al., 2014; Hartman et al., 2016). Shells from organisms such as gastropods and other mollusks are abundant in the fossil record and can be subsampled to produce stable isotope records along the direction of their growth. The stable isotope ratios in shell carbonate ($\delta^{18}O_{shell}$ and $\delta^{13}C_{shell}$) vary as the animal grows due to changes in temperature and changes in $\delta^{18}O_{water}$ values and $\delta^{13}C$ of dissolved inorganic carbon (DIC) in the freshwater environment (Leng and Marshall, 2004). Snails of the genus *Melanopsis* occur in freshwater bodies in the Mediterranean region and are common in the Levant, including the Hula Valley (Tchernov, 1973; Glaubrecht, 1993; Heller et al., 2005). Modern snails of this genus occur as far north as Hungary but are presently limited to thermal springs in that area (Glaubrecht, 1993). Life span estimates for this genus vary widely. Elkarmi and Ismail (2006) measured and weighed *Melanopsis* snails at Azraq Oasis, Jordan, and found five size

groups, estimating an age of 5 years for the largest snails. Zaarur et al. (2016) reported sclerochronological $\delta^{18}O_{shell}$ values from modern specimens in the Jordan River valley that reflect two seasonal cycles. Geary et al. (2012) suggest a much longer life span for specimens from paleo-Lake Pannon, with one individual surviving to 16 years based on sclerochronological evidence. Growth rates of these snails can differ based on environmental conditions, with warmer waters generally more favorable to growth and shell growth potentially slowing or pausing during the winter months (Geary et al., 2012; Bartolini et al., 2017).

The objective of our study is to use high-resolution sclerochronological $\delta^{18}O_{shell}$ and $\delta^{13}C_{shell}$ data from *Melanopsis* shells in a well-dated geoarchaeological sequence in the northern Jordan River valley to provide insight into hydrology, seasonality, and climate in the eastern Mediterranean during the late Pleistocene.

STUDY AREA

Geologic and hydrological setting

The Hula Basin is a small pull-apart basin associated with the Dead Sea Transform (Horowitz, 1973; Rybakov et al., 2003; Schattner and Weinberger, 2008; Heimann et al., 2009). The basin's area is approximately 150 km², and it serves as an erosion base level for approximately 1500 km². The valley floor is currently at an elevation of approximately 70 m above sea level (m asl). The basaltic Golan Heights plateau lies to the east, with Mt. Hermon (2814 m asl) marking the northeastern end of the region and the limestone mountains of the Upper Galilee bordering the west. The Kurazim uplifted basaltic block is the southern boundary of the basin. Subsidence has allowed sediments in the Hula Basin to accumulate since at least the middle to late Miocene (Rybakov et al., 2003).

The Hula Valley is the uppermost basin in the Jordan River catchment, where the Dan, Banias, and Hasbani Springs contribute the majority of the Jordan River headwaters. Precipitation in the Mt. Hermon area recharges these karst springs (Babad et al., 2020), with a snowmelt contribution of about 30% (Gil'ad and Bonne, 1990; Sade et al., 2016). Springs in the basaltic Golan Heights to the east of the valley also contribute to the Jordan River and may have played a larger role in the geologic past (Spiro et al., 2011). Attempts to better understand hydrogeology in the Hula Basin are complicated by its complex geology and a lack of wells and boreholes from which data can be collected. However, recent studies suggest surface discharge of deep groundwater in the southern part of the basin (Babad et al., 2020).

Before drainage in the 1950s, the Hula Valley held a shallow, up to 3-m-deep lake (~14 km²) at its southern end and extensive swamps to the north (Dimentman et al., 1992). Some wetlands were restored in the Agamon Hula Nature Reserve between 1994 and 2010. The reflooded area contains a small, shallow human-made lake fed by canals (Gophen et al., 2003). Hydrology of the Agamon Hula is seasonal, with rainy months raising the water level and dry months lowering the water level through evaporative loss (Gophen et al., 2003; Litaor et al., 2008).

Climate

The Hula Basin holds the headwaters of the Jordan River, the primary water source for the entire Dead Sea Rift valley. Modern climate is characterized by moderately cool, wet winters,

with mean January temperatures of about 12°C, and hot, dry summers, with mean July temperatures of 28°C. Mean annual temperature is 21°C, and annual rainfall ranges from 400 to 800 mm, with the northern end of the basin receiving significantly more precipitation than the southern end (van Zeist et al., 2009; Sade et al., 2016). Higher altitudes experience a cooler, wetter climate, with mean annual temperatures in the mountains and plateaus surrounding the Hula Basin reaching 16°C and a mean annual precipitation up to 1300 mm (Rimmer and Salingar, 2006; van Zeist et al., 2009; Sade et al., 2016).

Archaeological site

The Jordan River Dureijat excavation site (JRD; Fig. 1) lies on the eastern bank of the Jordan River at the confluence of the small Dureijat (meaning "steps" in Arabic) stream at the southern edge of the Hula Basin (Marder et al., 2015; Sharon et al., 2020). The site was discovered in 1999 during an archaeological survey before a Jordan River drainage operation. Excavation at the site continued with seven excavation seasons from 2014 to 2021 (Sharon et al., 2020). Sediments at the site are composed of silt layers indicating a submerged shallow lake environment and layers rich in gastropod and *Unio* shells representing a shallow nearshore lake environment (Sharon et al., 2020; Fig. 2).

The long and continuous record of archaeological remains at JRD is rare for the EP of this region. The archaeological sequence of JRD comprises almost the entire Levantine EP era (Goring-Morris and Belfer-Cohen, 2017), including an Early EP lithic tradition, the Middle EP Geometric Kebaran, and the three upper horizons documenting the Late EP Natufian cultural entity. In addition, evidence for Pre-Pottery Neolithic A presence was found in the uppermost archaeological layer of the JRD sequence. A rich assemblage of fishing gear exposed in all archaeological horizons documents more than 10,000 years of intermittent visits to the shore of paleo-Lake Hula (Sharon et al., 2020). Similar to other sites on the banks of the upper Jordan River (Goren-Inbar et al., 2002a, 2002b; Aharonovich et al., 2014; Melamed et al., 2016), waterlogged layers result in exceptional preservation of botanical remains and other paleoenvironmental proxies, which rarely occurs in EP sites in the region (Belfer-Cohen and Goring-Morris, 2013). The long and well-dated archaeological and sedimentological sequence of JRD, the exceptional preservation of paleoenvironmental proxies, its location in the core area of the Mediterranean Levantine EP, and its proximity to other key sites documenting the shift to sedentism and Neolithization together with its geographic location at the uppermost basin of the Jordan River valley, all make JRD an ideal location to study changing paleoenvironments and their impact on key changes in human history (Langgut et al., 2021).

MATERIALS AND METHODS

Shells from the JRD Area B east section (the type section of the site; Sharon et al., 2020; Fig. 2) were systematically collected during sediment logging in the 2016 and 2017 excavation seasons. The lowermost layer exposed at the east section (Layer 6) is ^{14}C dated as slightly older than 20 cal ka BP. The uppermost layer (Layer 3-0) is assigned to the beginning of the Holocene at 10.9 cal ka BP (Sharon et al., 2020). The sampled layers were chosen from among the sedimentary horizons bearing archaeological material across the chronological sequence and based on the presence of large, well-preserved shells (Fig. 2; Table 1).

Figure 1. (a) Eastern Mediterranean region and location of Jordan River Dureijat archaeological site (JRD; orange star). (b) Study area showing the location of JRD (orange star), Agamon Hula, Gesher Benot Ya'aqov (GBY), and nearby locations referenced in the text. The approximate outline of Lake Lisan during its LGM high stand is based on Torfstein et al. (2013).

A comparative control sample of live *Melanopsis* specimens documenting present-day conditions was collected from Agamon Hula in May 2017 and placed in ethanol. The largest shell in the sample was chosen for analysis. The shell was sandblasted to remove the periostracum, then cleaned with deionized water and a brush and needle to remove stains. It was then dried in an oven at 40°C.
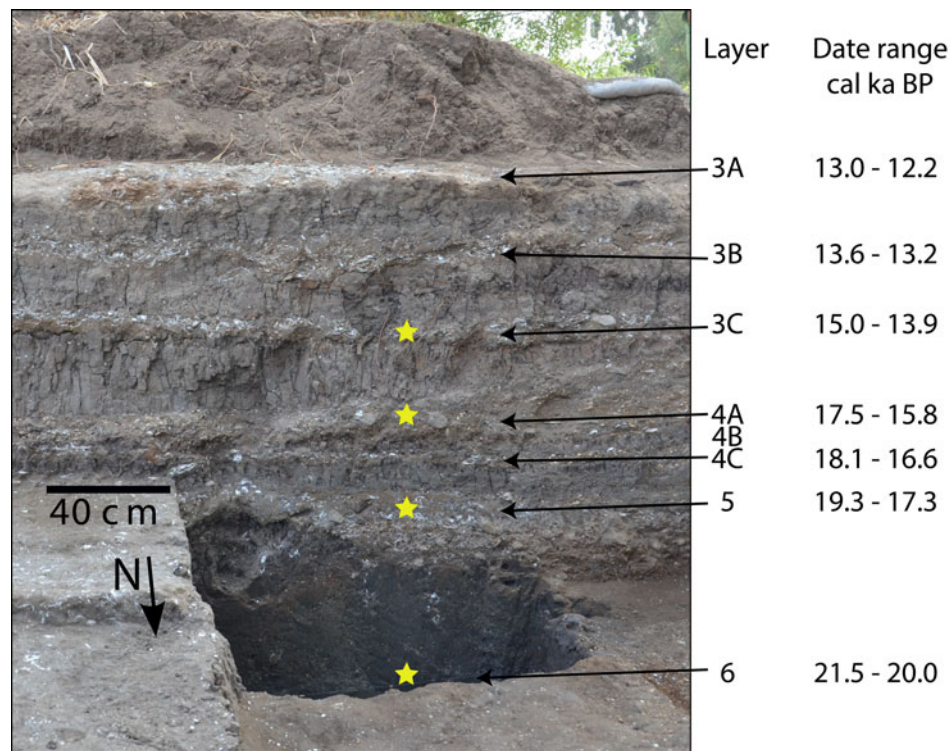
Figure 2. Stratigraphy and radiocarbon ages at Jordan River Dureijat archaeological site (JRD; adapted from Sharon et al., 2020). Yellow stars indicate the approximate depth of shells sampled for this study.

The chosen subfossil shells were placed in ethanol in an ultrasonic bath for 30 minutes. After drying at room temperature, the shells were cleaned with deionized water and a brush and needle and then dried in an oven at 40°C. After cleaning, all shells were photographed and whorls were counted. Locations of growth marks and areas of damage, staining, and poor preservation were noted. Species taxonomy was determined after Heller et al. (2005).

Samples were milled from the shell surface using a modified dental drill placed in a custom holder after Wiese et al. (2020). The apparatus was placed under a microscope to enable precise milling. A maximum milling depth of 50 µm was set using a gauge on the holder to ensure that only the outermost shell was sampled. Before each sample was milled, 5% HCl was applied to the drill bit and holder using a synthetic swab to remove carbonate contaminants, then deionized water was applied in the same manner to neutralize the surface. Finally, a pressurized air hose was used to dry the apparatus before use. Samples were milled using a 0.5-mm-round diamond bit, except for samples taken from the smallest whorls of Layer 3C Shell 1 and Layer 4 Shell 2. The heights of these whorls were smaller than 0.5 mm and required a tapered diamond drill bit. Shells were milled to collect 30–80 µg from the uppermost (oldest) whorls of all shells and 100–200 µg on larger whorls.

Each shell was individually assessed to determine appropriate sample spacing to collect 50 samples per shell. This number

Table 1. Shell size and archaeological layer ages and IDs reported by Sharon et al. (2020).[a]

Layer	Shell	Height (cm)	Diameter (cm)	Whorls	Ribs	Age (cal ka BP)	JRD sample code	m asl
N/A	Modern	1.78	0.79	7.75	Present	Modern	N/A	N/A
3C	Shell 1	1.70	0.66	7.50	Absent	14.96–13.88	JRD16-099	56.99
3C	Shell 2	1.62	0.68	7.50	Present	14.96–13.88	JRD16-099	56.99
4	Shell 1	2.56	1.04	7.75	Absent	17.46–15.75	JRD16-128	56.66
4	Shell 2	2.42	1.00	7.00	Absent	17.46–15.75	JRD16-128	56.66
5	Shell 1	1.86	0.78	7.00	Present	19.30–17.30	JRD17-432	56.27
5	Shell 2	1.43	0.66	6.00	Present	19.30–17.30	JRD17-432	56.27
6	Shell 1	1.81	0.73	7.50	Faint	>20	JRD17-517	55.34
6	Shell 2	1.90	0.80	6.50	Faint	>20	JRD17-517	55.34

[a]JRD, Jordan River Dureijat archaeological site; m asl, meters above sea level.

allows for a submonthly sampling resolution for an assumed life span of 2 years. Degraded or stained areas were avoided to the extent possible. Due to size constraints, 45 samples from Layer 5 Shell 2 were collected. Because of shell damage during sampling, 48 samples were collected from Layer 3C Shell 2.

To determine the preservation state of the shells, the microstructures of a shell from Layer 5 and another shell from Layer 3C were examined with a Hitachi TM3000 desktop scanning electron microscope (SEM) at University of Iceland. Shell subsamples of ca. 2 mm^2 size were broken off the shells, coated with gold, and visually inspected. Examination with the SEM revealed the presence of crossed-lamellar layers (Iljina and Frolov, 2010; Supplementary Fig. 1). Signs of microbial attack or diagenetic shell alteration were not observed; thus, the material was considered to be reliable.

Oxygen and carbon isotope ratios were determined from 30–80 µg aliquots of sample material using a Thermo Scientific KIEL IV Carbonate Device coupled to a MAT 253 isotope ratio mass spectrometer at the GFZ Potsdam, Germany. The system, reference gas, and internal standard C1 were routinely calibrated against the Vienna PeeDee Belemnite (VPDB) standard using the international reference materials NBS19 ($\delta^{13}C = 1.95‰$, $\delta^{18}O = -2.2‰$) and NBS18 ($\delta^{13}C = -5.014‰$, $\delta^{18}O = -23.2‰$). The measured sample data were adjusted using the calibrated internal laboratory standard C1 ($\delta^{13}C = 2.40‰$, $\delta^{18}O = -1.31‰$), which was run six times between 40 samples. Repeated measurements of NBS19 and C1 standard material show a precision better than ±0.08‰ and for NBS18 better than ±0.1‰ for both $\delta^{13}C$ and $\delta^{18}O$. To correct for acid fractionation of aragonite, −0.38‰ offset was applied after Kim et al. (2007a). Isotope ratios of shells are reported in the delta notation relative to VPDB, and the cited and calculated oxygen isotope values of water ($\delta^{18}O_{water}$) are expressed relative to Vienna Standard Mean Ocean Water (VSMOW).

Due to low intensities in the smallest samples of the upper whorls, $\delta^{13}C$ and/or $\delta^{18}O$ values for 39 samples could not be determined. An additional seven samples were milled and analyzed where possible. Two split samples were analyzed, Modern Shell (sample 49) and Layer 4 Shell 2 (sample 16). Based on the results, an overall uncertainty of 0.2‰ is assumed for this study. The $\delta^{18}O$ and $\delta^{13}C$ values are reported to 0.1‰ precision. All shells were photographed after milling to document sample locations (Rice, 2018).

Interpretation framework for $\delta^{18}O$ and $\delta^{13}C$ profiles

As gastropods precipitate their shells, the $\delta^{18}O_{shell}$ values primarily reflect those of the lake water and an offset due to temperature effects (Schmitz and Andreasson, 2001; Spiro et al., 2009). Precipitation, evaporation, and inflowing water can alter $\delta^{18}O_{water}$ in the snail's habitat. Evaporation leads to higher $\delta^{18}O_{water}$ values in the lake, while the input of freshwater in the form of precipitation or inflow typically leads to lower values (Leng and Marshall, 2004). Meltwater from snow and rainwater that falls at high altitudes to recharge springs can contribute to low $\delta^{18}O_{water}$ values in the Jordan River (Gat and Dansgaard, 1972; Zaarur et al., 2016). In addition, some storms can bring high-$\delta^{18}O$ rainwater. Sub-cloud evaporation of raindrops and convective rain that originates from evaporated water over land will result in high $\delta^{18}O_{water}$ values in rain (Gat and Dansgaard, 1972). Offsets in $\delta^{18}O_{shell}$ values due to temperature are often smaller than the changes in evaporation and precipitation in a

lacustrine environment. Specifically, increases in temperature lead to lower $\delta^{18}O_{shell}$ values but to increased evaporation, which results in higher $\delta^{18}O_{water}$ values. Because $\delta^{18}O_{shell}$ values change by only 0.24‰/°C (Kim et al., 2007b), the changes in $\delta^{18}O_{water}$ values due to evaporation are often more important. Similarly, colder temperatures lead to higher $\delta^{18}O_{shell}$ values but coincide with the rainy season, which leads to lower $\delta^{18}O_{water}$ values in the lake. It is possible that subfossil shells grew during intervals of lower evaporation, in which case temperature effects on $\delta^{18}O_{shell}$ values might be more important. In this case, decreasing $\delta^{13}C_{shell}$ values are still expected with lowering temperatures due to decay of organic matter, and we rely on $\delta^{13}C_{shell}$ values to indicate possible pauses in growth during winter.

Meanwhile, $\delta^{13}C_{shell}$ values will reflect the $\delta^{13}C_{DIC}$ values in the water. In lake water, $\delta^{13}C_{DIC}$ values are impacted by the $\delta^{13}C$ values of inflowing DIC, exchange with the atmosphere, and photosynthesis and respiration of aquatic plants (Leng and Marshall, 2004). Aquatic productivity is generally the most important factor on short (subannual) timescales and leads to increased values of $\delta^{13}C_{DIC}$ in the lake, whereas the decay of organic matter leads to lowered values of $\delta^{13}C_{DIC}$ (Leng and Marshall, 2004). Storms wash soil into the lake, bringing low-$\delta^{13}C$ carbon into the lake system.

Growth marks can also aid in interpreting the $\delta^{18}O_{shell}$ and $\delta^{13}C_{shell}$ profiles. Growth marks indicate an interval when the gastropod pauses its shell growth, which may occur for several reasons. Changes in the environment, including changes in temperature or turbidity, can induce growth marks, but reproduction can also result in a pause in shell growth (Schöne et al., 2007; Mannino et al., 2008; Geary et al., 2012). Some studies have noted the formation of these features during times of thermal stress, both for cold and hot temperatures (Schöne et al., 2007; Mannino et al., 2008). Gastropods may respond to thermal stress by thickening their shell rather than lengthening it in order to improve insulation (Mannino et al., 2008). The duration of time represented by growth marks varies; while one growth mark could represent an entire wet season, another might represent a pause in growth for a much shorter interval.

When a growth mark coincides with a decrease in $\delta^{13}C_{shell}$ values, this event is interpreted as a pause in growth during winter months, with changing $\delta^{13}C_{DIC}$ values due to decay of aquatic organic matter during winter. However, storms can also cause this same pattern, where the water may become turbid, inducing a pause in growth when low-$\delta^{13}C$ soil is washed into the lake. For growth marks preceded by several samples with elevated $\delta^{13}C_{shell}$ values or a long trend toward higher $\delta^{13}C_{shell}$ values, the growth mark likely represents winter. Growth marks that coincide with a drop in $\delta^{13}C_{shell}$ values without any long trend beforehand could be attributed to either a storm or to winter. For shells where this occurs early in life, it is particularly difficult to discern due to the small time span represented by each sample. In addition, samples collected from the last part of the shell to precipitate may represent longer intervals of time due to slower growth rates later in the snail's life. This area can also contain several growth marks due to reproduction (Geary et al., 2012). So, the samples collected from this part of the shell are likely to represent averages of several weeks or even months, and growth marks are less likely to represent winter than in earlier parts of the shell.

After the growth marks likely to represent winter are identified, the $\delta^{18}O_{shell}$ values are interpreted as changes in $\delta^{18}O_{water}$ and temperature. Decreases in $\delta^{18}O_{shell}$ values result from the input of low-$\delta^{18}O$ water into the lake, either through direct

Table 2. Summary statistics of $\delta^{18}O$ and $\delta^{13}C$ values (‰).

Shell name	$\delta^{18}O$ min.	$\delta^{18}O$ max.	$\delta^{18}O$ mean	$\delta^{18}O$ SD	$\delta^{13}C$ min.	$\delta^{13}C$ max.	$\delta^{13}C$ mean	$\delta^{13}C$ SD
Modern	−9.39	−3.41	−6.73	1.61	−8.60	0.46	−4.54	2.96
Layer 3C Shell 1	−7.46	−4.61	−6.42	0.65	−7.08	−2.20	−4.33	1.27
Layer 3C Shell 2	−7.72	−4.70	−6.66	0.68	−7.39	−2.63	−4.17	1.21
Layer 4 Shell 1	−8.73	−5.28	−7.59	0.71	−8.27	−4.07	−6.44	1.15
Layer 4 Shell 2	−9.35	−5.70	−7.86	0.82	−8.02	−4.78	−6.41	0.74
Layer 5 Shell 1	−7.88	−5.53	−6.92	0.59	−9.42	−6.27	−7.65	0.77
Layer 5 Shell 2	−8.22	−5.65	−7.32	0.62	−8.62	−6.43	−7.39	0.49
Layer 6 Shell 1	−7.92	−4.93	−7.04	0.57	−9.05	−4.84	−6.59	0.97
Layer 6 Shell 2	−9.03	−5.19	−7.36	0.69	−8.53	−5.68	−6.58	0.66

precipitation, inflow, runoff, or snowmelt. Temperature increases can also result in decreases in $\delta^{18}O_{shell}$ values; however, temperature is likely to be a relatively minor effect, with a temperature increase of 4°C resulting in a decrease in $\delta^{18}O_{shell}$ of about 1‰ (Kim et al., 2007b). Trends toward higher $\delta^{18}O_{shell}$ values generally indicate ^{18}O enrichment of lake water due to evaporation in summer months. High-$\delta^{18}O$ rainfall can also raise $\delta^{18}O_{lake}$ values. In the modern climate, this occurs due to sub-cloud evaporation of raindrops or due to convective precipitation, where the cloud's moisture source originated on land. In addition, hydrological conditions during the LGM may have led to a greater proportion of snow recharge to the headwater springs, leading to higher $\delta^{18}O_{water}$ values of winter rainfall within the valley compared with summer lake water fed by the springs, which are recharged by low-$\delta^{18}O_{water}$ snowmelt. Elevated values of $\delta^{18}O_{shell}$ immediately following the winter growth mark may indicate high values of $\delta^{18}O_{water}$ during winter compared with summer, likely indicating the effect of snowmelt on $\delta^{18}O$ of river recharge.

Although two shells were subsampled per sediment interval, it is unlikely that the shells grew in the same years. Each shell likely represents distinct intervals of time, and due to interannual variability in temperature and precipitation, the conditions of growth differ from one specimen to another. Nevertheless, two shells from the same layer, despite differences in timing of, for example, storms, should display similar, likely typical conditions of the climate in which they grew. Although climate is defined based on multi-decadal averages, it is unlikely that two shells from a sedimentary interval spanning about 23–70 years would both record the same unusual conditions occurring in consecutive years of growth. The likelihood of, for example, a 25 year flood event occurring at least once during a 2 year interval of shell growth is 8%. The likelihood for two independent 25 year events to occur in two sequential years is only 0.16%.

Modeling $\delta^{18}O_{shell}$ patterns

The ShellChron model package (de Winter, 2022) includes a script to generate a modeled $\delta^{18}O_{shell}$ record from sinusoidally varying temperature and $\delta^{18}O_{water}$ curves, which was used to validate the data generated from the modern shell assessed in this study and from modern shells in nearby locations analyzed by Zaarur et al. (2016). Temperature and $\delta^{18}O_{water}$ values reported in the literature were used to generate this record (Gat, 1970; Gat and Dansgaard, 1972; Gil'ad and Bonne, 1990; Litaor et al.,

2008; Gophen et al., 2016; Zaarur et al., 2016; Supplementary Text S1). To mimic weather effects, model temperature and $\delta^{18}O_{water}$ values vary randomly within a normal distribution from the seasonal curve, calculated with standard deviations of 1.5°C and 0.6‰ from the seasonal model temperature and $\delta^{18}O_{water}$ values, respectively. The code was adapted to use the Kim et al. (2007b) temperature-dependent oxygen isotope relationship between aragonite and the water from which it precipitates:

$$1000 \ln \alpha = 17.88 \times 10^3/T - 31.14 \qquad (Eq.1)$$

where $\alpha = (\delta^{18}O_{shell} + 1000)/(\delta^{18}O_{water} + 1000)$. Solving for $\delta^{18}O_{shell}$:

$$\delta^{18}O_{shell} = (\delta^{18}O_{water} + 1000) \times e^{(17.88 \times 10^3/T - 31.14)/1000}$$
$$- 1000 \qquad (Eq.2)$$

Values from Eq. 2 yield $\delta^{18}O_{shell}$ values in the VSMOW reference frame, which are then converted to VPDB for comparison with measured $\delta^{18}O_{shell}$ data.

To mimic pauses in growth during winter months, a temperature cutoff value of 14.5°C was implemented under which the shell is assumed not to grow. This cutoff value was determined using the modern shell models and fit to better reflect patterns in the modern shells; it is assumed to be the same for all shells.

The model shell module was also used to assess the plausibility of different temperature and $\delta^{18}O_{water}$ regimes in fossil shells. The temperature and $\delta^{18}O_{water}$ inputs were fit to shell results. Rather than attempting to model each variation in each shell, the overall variability of $\delta^{18}O_{shell}$ data was fit for each paleoclimate interval.

RESULTS

Fossil shells from JRD are identified as *Melanopsis buccinoidea* (no ribs) or *Melanopsis costata* (ribbed specimens; Heller et al., 2005). However, whether these morphological differences constitute a separate species in Levantine *Melanopsis* is under dispute (Falniowski et al., 2020). The large shells selected for analysis are consistent with observed sizes of adult specimens, ranging in length from 1.43 to 2.56 cm and in diameter from 0.66 to 1.04 cm, and having between 6.00 and 7.75 whorls (Table 1). All shells contained multiple growth marks, some of which are faint and others more readily visible. The duration of interpreted

growth cessation based on sclerochronological evidence was not apparent based on the visual appearance of these marks.

Sclerochronological $\delta^{18}O_{shell}$ and $\delta^{13}C_{shell}$ results are provided in Supplementary Table 1. Means of sclerochronological $\delta^{18}O_{shell}$ and $\delta^{13}C_{shell}$ values for each shell range from −7.9 to −6.4‰ and −7.7 to −4.2‰, respectively. The smallest range of $\delta^{18}O_{shell}$ values, 2.3‰, was calculated for Layer 5 Shell 1, and the largest range, 6.0‰, for the modern shell (Table 2). The $\delta^{13}C_{shell}$ values fluctuate by 2.2‰ at their minimum (Layer 5 Shell 2) and by 9.1‰ at their maximum (modern shell). Detailed shell interpretations based on the framework outlined earlier are given in Supplementary Text S2). These are briefly described in the following section and shown in Figure 3.

Shell sclerochronology interpretations

The modern shell from Agamon Hula has large changes in $\delta^{18}O_{shell}$ values consistent with a large evaporation effect (Fig. 3a). Winter growth marks (G and H) are identified as the largest decreases in $\delta^{18}O_{shell}$ and $\delta^{13}C_{shell}$ values. Two annual cycles are inferred, each of which shows a trend toward high $\delta^{18}O_{shell}$ values with a bifurcated peak that may have come about due to artificial water level adjustment. One inferred storm event occurs in the first year of growth, which may correspond to an April 2015 storm (Israel Meteorological Service, 2018; Supplementary Fig. 2). Although another storm occurred in April 2016, the impact of this storm on Agamon Hula $\delta^{18}O_{water}$ values is not observed.

The shells from Layer 3C have large and concurrent decreases in $\delta^{18}O_{shell}$ and $\delta^{13}C_{shell}$ values that indicate winter (Shell 1 growth marks B and C; Shell 2 growth marks A and D), but show more gradual increases in $\delta^{18}O_{shell}$ values compared with $\delta^{13}C_{shell}$ values (Fig. 3b and c). Layer 3C Shell 1 records two clear annual cycles and has two additional large decreases in $\delta^{13}C_{shell}$ values (growth marks E and I) that could indicate either winter season or storm events. Layer 3C Shell 2 contains a large damaged portion where the surface layer of the shell flaked off upon contact and which was not sampled for stable isotope analysis. In the remainder of the shell, two annual cycles are inferred (winter growth marks A and D), with one major event that lowered $\delta^{13}C_{shell}$ values and increased $\delta^{18}O_{shell}$ values in the second annual cycle (growth mark B). This event may have been another annual cycle and winter growth mark; however, the small area of the shell that these samples represent suggests that this was a storm event.

Shells from Layer 4 exhibit large, rapid changes in $\delta^{18}O_{shell}$ and $\delta^{13}C_{shell}$ values (Fig. 3d and e). The frequency and timing of changes in $\delta^{18}O_{shell}$ and $\delta^{13}C_{shell}$ values and the lack of a clear relationship between these changes make it difficult to reliably discern annual cycles. The complexity in the patterns could be the result of more frequent storms, interannual variability in the source or amount of rain, or variability in $\delta^{13}C_{DIC}$ values due to processes other than aquatic productivity and decay, such as input of soil carbon from wind erosion and storm runoff. Growth marks concurrent with decreases in $\delta^{13}C_{shell}$ values occur six times in Layer 4 Shell 1 (growth marks A, B, E, G, I, and J) and four times in Shell 2 (growth marks B, D, E, and F). These are interpreted as winter growth marks. Trends toward lower $\delta^{18}O_{shell}$ values occur after these marks, which could be due to either increased temperature or lower $\delta^{18}O_{water}$ values during summer.

In Layers 5 and 6, minima in $\delta^{13}C_{shell}$ values generally coincide with peaks in $\delta^{18}O_{shell}$ values (Fig. 3f–i). Winter growth marks identified by decreases in $\delta^{13}C_{shell}$ values occur three times in Layer 5 Shells 1 (growth marks A, E, and F) and 2 (growth marks A, C, and D), twice in Layer 6 Shell 1 (growth marks B and C), and five times in Layer 6 Shell 2 (growth marks B, C, D, E, and G). Changes in $\delta^{18}O_{shell}$ values are generally gradual, with some exceptions that may indicate storms: Layer 5 Shell 1 before growth mark D; Layer 6 Shell 1 before growth mark E; and Layer 6 Shell 2 before growth marks B and G.

Shell isotope models

Models of $\delta^{18}O_{shell}$ values for the modern Jordan River and Sea of Galilee reflect the general range of measured $\delta^{18}O_{shell}$ values. However, the modeled Dan Spring shell has a larger deviation from measured values (−8.3 to −6.1‰ modeled vs. ∼ −7.2 to −6.3‰ measured; Zaarur et al., 2016), and the modeled Agamon Hula shell also has a different range than measured values (−7.1 to −2.9‰ modeled vs. ∼ −8.4 to −3.4‰ measured). It is possible that the modeled temperature or $\delta^{18}O_{water}$ used in these scenarios does not appropriately describe the conditions under which the shells grew. Given these discrepancies, the $\delta^{18}O_{water}$ in fossil scenarios is estimated to vary within ±1‰ of modeled results. When parts of the model shell that formed below 14.5°C are removed, model results closely resemble patterns in measured $\delta^{18}O_{shell}$ values (Fig. 4).

Water temperature and $\delta^{18}O_{water}$ parameters that best fit fossil shell patterns (Table 3) suggest that $\delta^{18}O_{water}$ values were seasonally highest at the end of the evaporative summer season in Layer 3C shells, but shells formed in Layers 4–6 exhibit patterns that are better explained by higher $\delta^{18}O_{water}$ values during cold conditions. Furthermore, seasonal amplitudes of modeled $\delta^{18}O_{water}$ values are higher for the Bølling-Allerød (2.6‰) compared with Heinrich 1 and the LGM (1.8‰ and 0.8‰, respectively). Resulting modeled $\delta^{18}O_{shell}$ patterns closely resemble typical patterns in the shells after removing parts of the model shell that formed below 14.5°C (Fig. 4).

DISCUSSION

Modern shells

Oxygen isotope variations within modern *Melanopsis* shells from Agamon Hula (this study), Dan Spring, the Jordan River, and the Sea of Galilee (Zaarur et al., 2016) exhibit seasonal fluctuations in magnitudes consistent with their environments. Of these, Dan Spring is the least seasonally varying environment in terms of water temperature (1°C) and $\delta^{18}O_{water}$ values (1‰) and exhibits the narrowest range of seasonal $\delta^{18}O_{shell}$ values (∼1.2‰). Variations in $\delta^{18}O_{shell}$ values from the Sea of Galilee, Jordan River, and Agamon Hula shells are increasingly variable due to higher variability in their environments. The general agreement between modeled shells and measured $\delta^{18}O_{shell}$ values also suggests that the oxygen isotope values in the shells faithfully record changes in the environment, as has been found for other freshwater gastropods (Schmitz and Andreasson, 2001; Spiro et al., 2009). A strict temperature cutoff of 14.5°C imperfectly describes *Melanopsis* shell growth. The patterns of modeled $\delta^{18}O_{shell}$ values above this cutoff seem to replicate conditions in Agamon Hula well; however, this cutoff is only rarely reached in the other modern environments. The shells assessed by Zaarur et al. (2016)
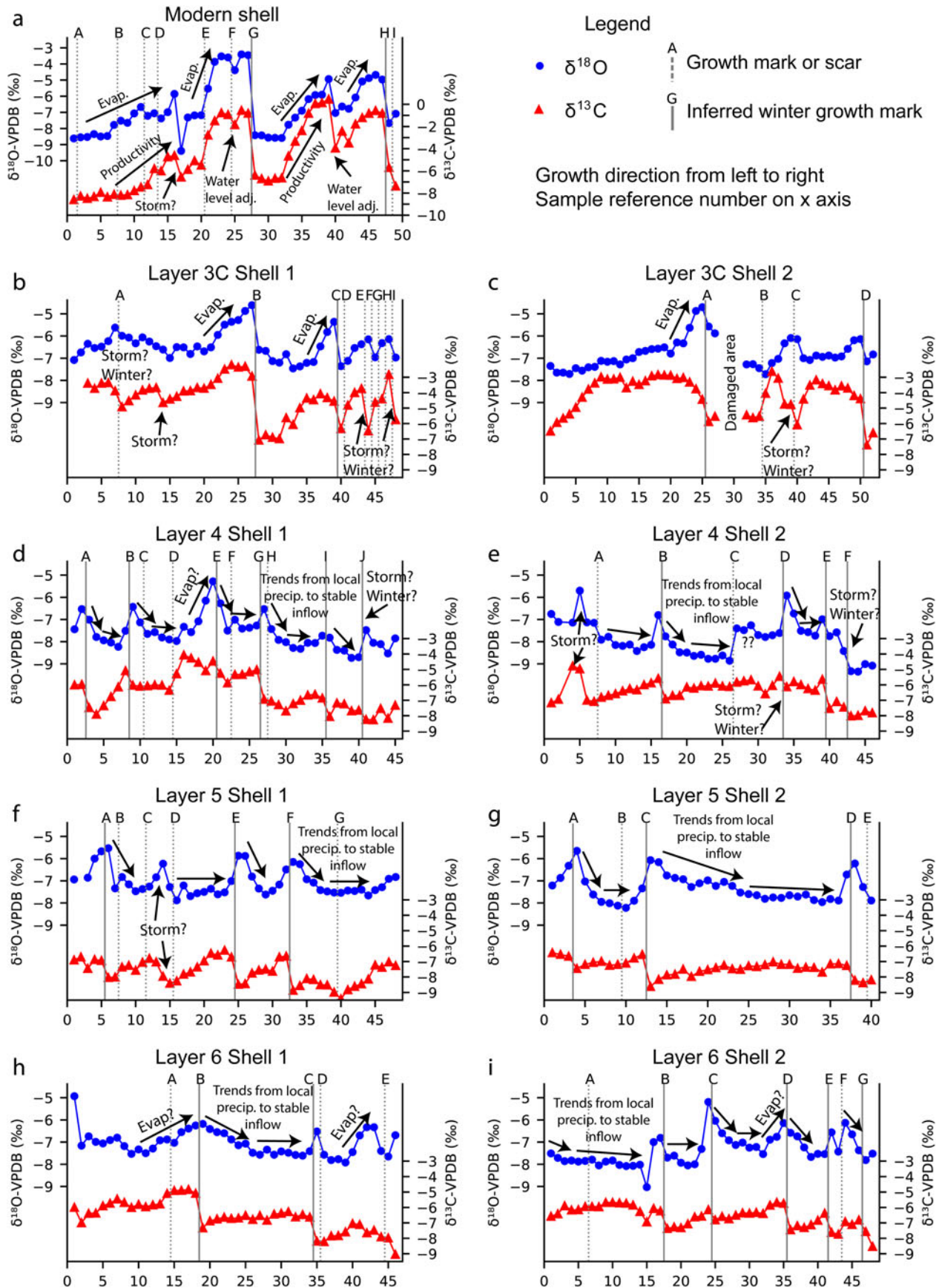
Figure 3. Sclerochronological results of $\delta^{18}O_{shell}$ (blue circles) and $\delta^{13}C_{shell}$ (red triangles) for the modern shell and subfossil shells annotated with environmental inferences. Growth marks (gray dashed lines) between samples are labeled with letters. Growth direction is from left to right.
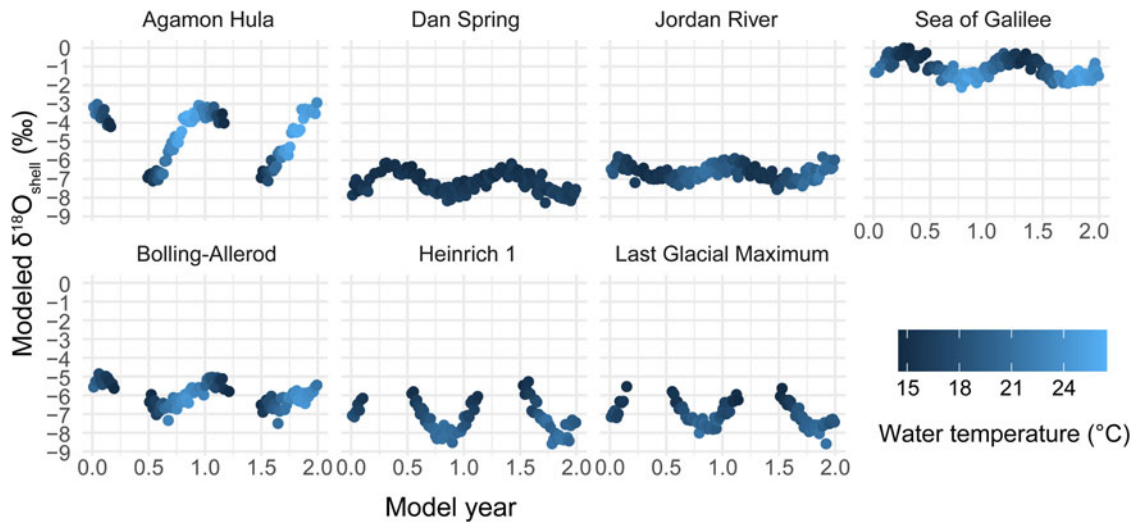
Figure 4. Model results of $\delta^{18}O_{shell}$ for modern (top) and paleo (bottom) scenarios.

exhibit sawtooth-shaped $\delta^{18}O_{shell}$ patterns, suggesting seasonal growth patterns with slow or paused growth in winter. Because temperatures below 14.5°C are rarely reached in these habitats, a strict temperature cutoff might not reflect actual growth conditions. Instead, these gastropods might slow growth during winter in relatively warm waters or might stop growth due to a nonthermal factor, such as storm-induced turbidity at the beginning of the wet season.

Although few *Melanopsis* shells from modern environments have been examined, model $\delta^{18}O_{shell}$ results suggest that the general variability within the gastropod's environment can be understood through the extent of seasonal variations in $\delta^{18}O_{water}$ values and, to a lesser extent, seasonal temperature variability. Due to model assumptions, short-term changes in $\delta^{18}O_{water}$ values cannot be replicated, and seasonal changes that are not purely sinusoidal have not been assessed. Due to the lack of subseasonal $\delta^{18}O_{water}$ measurements of modern water bodies, it remains open whether the oxygen isotope compositions follow a sinusoidal curve. Because of these limitations in robustly reconstructing growth rates, inferences of the paleoenvironment are focused on general seasonal patterns and the frequency of inferred storms.

Paleohydrological and paleoclimate inferences

With two to five annual growth cycles, an individual specimen provides a subsample of climate that may not be fully representative of the long-term mean, range, and extremes. As a result, interpretation of the data as typical for climate conditions during the interval of shell growth is tentative. However, assessing two shells per interval and comparing trends makes it relatively unlikely that only unusual years are represented by studied materials. Within each layer, the stable isotope patterns generally agree between and within shells, suggesting that the shells and the cycles within them represent conditions typical of the stratigraphic interval. Furthermore, with the exception of Layer 4 shells, annual cycles within a shell usually vary between the same high and low $\delta^{18}O_{shell}$ values, showing seasonality that repeats itself in adjacent years. Higher variability in Layer 4 shells could point to greater interannual variability within the waterbody during the Heinrich 1 event. This would be in agreement with pollen-based biome modeling that suggests more frequent summer rainfall (Langgut et al., 2021), which possibly led to stable isotope patterns with less regularity. In the present climate, small, localized summer storms occur in northern Israel without

Table 3. Model temperature, $\delta^{18}O_{water}$, and $\delta^{18}O_{shell}$ parameters and comparison with measured $\delta^{18}O_{shell}$ values.

| Model shell	Water temperature range		$\delta^{18}O_{water}$ range (‰)		Day max. $\delta^{18}O_{water}$	Model $\delta^{18}O_{shell}$ range (>14.5°C)		Measured $\delta^{18}O_{shell}$ range (‰)	
Modern scenarios									
Agamon Hula	11.0	26.0	−7.7	−1.7	190	−7.1	−2.9	−8.4	−3.4
Dan Spring	15.1	16.1	−8.0	−7.0	50	−8.3	−6.1	−7.2	−6.4
Jordan River	15.0	21.0	−7.25	−5.75	190	−7.6	−5.8	−7.7	−6.0
Sea of Galilee	15.0	25.0	−1.25	0.25	190	−2.1	0.0	−1.7	0.5
Paleo-Lake Hula scenarios									
Bølling-Allerød	12.0	24.0	−7.1	−4.5	190	−7.5	−4.9	−7.4	−4.9
Heinrich 1	11.0	21.0	−7.5	−5.7	50	−8.6	−5.3	−8.7	−5.9
Last glacial maximum	11.5	20.5	−7.1	−6.3	50	−8.6	−5.5	−8.2	−5.6
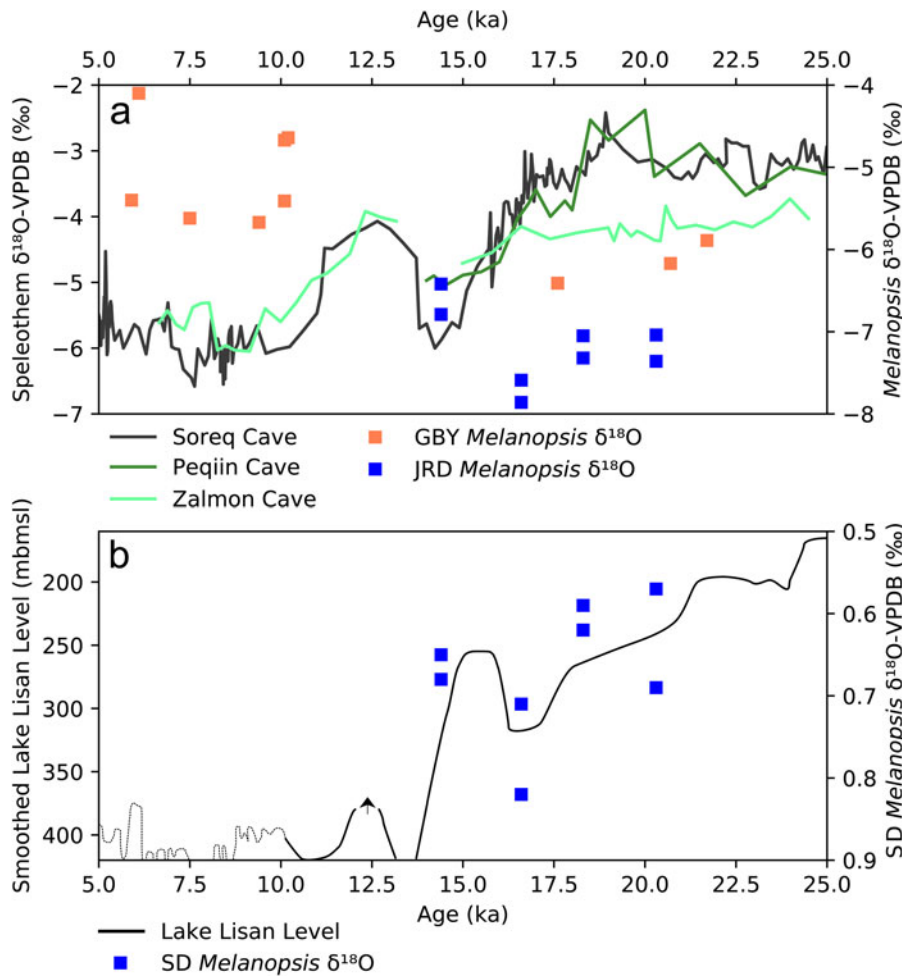
Figure 5. (a) A comparison of *Melanopsis* $\delta^{18}O_{shell}$ from this study (blue squares) and Zaarur et al. (2016; pink squares) to $\delta^{18}O_{speleothem}$ records from Soreq (gray), Peqiin (dark green), and Zalmon (light green) Caves (Bar-Matthews et al., 2003; Keinan et al., 2019) and (b) standard deviation of $\delta^{18}O_{shell}$ values in *Melanopsis* (blue squares; note the inverted axis) compared with the Lake Lisan lake level curve (Torfstein et al., 2013). GBY, Gesher Benot Ya'aqov; JRD, Jordan River Dureijat archaeological site.

disrupting the regional synoptic-scale forcing that causes dry summers (Saaroni and Ziv, 2000). Storms can lead to highly variable $\delta^{18}O_{water}$ values in the modern-day Jordan River (Gat and Dansgaard, 1972), with Hula Valley $\delta^{18}O_{precipitation}$ values reaching as low as −11‰ (Rindsberger et al., 1990), and similar storms may have had analogous effects in paleo-Lake Hula. The longer inferred life span (about 5.5 and 4.5 years) of these specimens increases the likelihood that these specimens experienced more atypical macroweather conditions. Storm events are also inferred for both Bølling-Allerød (Layer 3C) shells, whereas not all LGM shells (Layers 5 and 6) exhibit these features, which could be due to fewer storms during spring and autumn in this time interval or a shorter growing season. Pollen-based modeling suggests greater spring and autumn precipitation during the Bølling-Allerød (Langgut et al., 2021), in agreement with shell-based inferences.

Variations in whole-shell $\delta^{18}O$ values can provide further insight into environmental changes. Over the studied time interval, the average $\delta^{18}O_{shell}$ values exhibit an opposite trend to $\delta^{18}O_{speleothem}$ records from Soreq Cave and Peqiin Cave, in line with previous findings (Zaarur et al. 2016; Fig. 5a). However, while Zaarur et al. (2016) attribute low *Melanopsis* $\delta^{18}O_{shell}$ values during the LGM to increased snowfall, the summer growth bias observed in this study suggests that whole-shell averages may more closely reflect changes in summertime evaporation than changes in $\delta^{18}O$ values of winter precipitation. In the general trend of increasing $\delta^{18}O_{shell}$ values from the LGM to the

Holocene, this seems to fit expectations of greater summer evaporation due to increasing temperatures, which is thought to have controlled the water balance of Lake Lisan during this time interval (Stockhecke et al., 2016; Miebach et al., 2019; Langgut et al., 2021; Ludwig and Hochman, 2022). However, the shells from Heinrich 1 (Layer 4), during which lake levels dropped suddenly, have lower $\delta^{18}O_{shell}$ values than those from the LGM. Evidence suggests that this event resulted in cold and dry conditions, in which low precipitation likely caused the lake-level drop (Bar-Matthews et al., 2003; Bartov et al., 2003; Langgut et al., 2021). The cold conditions likely also resulted in low summer evaporation, though this has not yet been studied. Nevertheless, the overall pattern of increasing $\delta^{18}O_{shell}$ values indicating greater summer evaporation aligns with sclerochronological evidence from JRD, with highest $\delta^{18}O_{shell}$ values recorded by the shells from the Bølling-Allerød (Layer 3C).

The results of sclerochronological $\delta^{18}O_{shell}$ analysis suggest that fluctuations in lake level of paleo-Lake Hula mirror those in downstream Lake Lisan, providing evidence that much of the water feeding Lake Lisan flowed from the northern end of the catchment. During the LGM, variations in $\delta^{18}O_{shell}$ values are small, indicating a large, well-buffered waterbody at a time when Lake Lisan stood at a high stand (Bartov et al., 2002; Torfstein et al., 2013). After the LGM, Lake Lisan was lower, and lake levels dropped dramatically during Heinrich 1 (Bartov et al., 2003), when low water levels are also inferred at paleo-Lake Hula from highly fluctuating $\delta^{18}O_{shell}$ values. Lake

Lisan again rose, reaching high levels at about 15 ka, though not as high as LGM levels (Torfstein et al., 2013). At this time, the waterbody size at JRD was intermediate: neither as well-buffered as it was during the LGM nor as poorly buffered as during Heinrich 1. The qualitative agreement in lake size changes between paleo-Lake Hula at JRD and Lake Lisan provides further evidence that fluctuations in flow from the Hula catchment contributed to changes in lake level at Lake Lisan. Indeed, the standard deviation of $\delta^{18}O_{shell}$ values seems to vary with the Lake Lisan curve from Torfstein et al. (2013; Fig. 5b). When the standard deviation is low, $\delta^{18}O_{water}$ values in the lake exhibit little fluctuation and Lake Lisan levels are high, while greater standard deviations, reflecting large fluctuations in $\delta^{18}O_{water}$ values, coincide with lower levels of Lake Lisan. This is likely due to the buffering capacity of a larger lake, in which storms have lower impacts on $\delta^{18}O_{water}$ values due to mixing a small amount of water from a storm with a large amount of lake water. However, this relationship may not always hold true. Modeled $\delta^{18}O_{shell}$ values show that the timing of maxima in $\delta^{18}O_{water}$ values in relation to maxima in water temperature can impact the magnitude of variability in $\delta^{18}O_{shell}$ values. When summer evaporation leads to the highest $\delta^{18}O_{water}$ values in the lake, the seasonal extent of $\delta^{18}O_{shell}$ values is smaller than when the highest $\delta^{18}O_{water}$ values occur in winter. This is due to the temperature fractionation effect, in which increased temperatures lead to lower $\delta^{18}O_{shell}$ values at a given $\delta^{18}O_{water}$ value. This effect diminishes the peak $\delta^{18}O_{shell}$ values when high temperatures coincide with high $\delta^{18}O_{water}$ values. So, for environments in which evaporation controls $\delta^{18}O_{water}$ values and the highest $\delta^{18}O_{water}$ values occur during the hottest parts of the year, the seasonal variability in $\delta^{18}O_{shell}$ values will be smaller than for environments that experience a different seasonal regime. This complicates a direct comparison of variability in $\delta^{18}O_{shell}$ values from Layer 3C and other fossil layers.

Sclerochronological data of the LGM shells possibly support the inference of a greater proportion of snowfall in the nearby mountains (Develle et al., 2011; Orland et al., 2012; Ayalon et al., 2013; Zaarur et al., 2016; Moulin et al., 2022). At present, snow accumulates near the summit of Mt. Hermon during the winter season, and melt contributes about 30% of the water in karstic springs that feed the Jordan River (Gil'ad and Bonne, 1990; Sade et al., 2016). A consistent, strong negative $\delta^{18}O_{shell}$ excursion that could indicate a sudden influx of snowmelt to paleo-Lake Hula was not observed in the examined shells. Only one shell of four dated to the LGM exhibits a possible snowmelt signal (Layer 6 Shell 2 sample 15), which is not repeated in the next interpreted annual cycle. A similar anomalous event appears in the modern shell from Agamon Hula (sample 17), for which snow is not a likely cause. The sampling resolution was possibly not high enough to detect such a signal in other shells, or snowmelt may have occurred during the snail's winter growth hiatus. Another possibility is that snowmelt quickly entered the karstic aquifer near Mt. Hermon, similar to conditions today (Sade et al., 2016). This would contribute water with lower $\delta^{18}O$ values to the main springs feeding the lake, resulting in lower $\delta^{18}O_{water}$ values in summer due to recharge from snow-fed springs and higher $\delta^{18}O_{water}$ values during winter, when precipitation falls as rain in the Hula Valley. The patterns in $\delta^{18}O_{shell}$ values from Layers 4–6 closely resemble modeled $\delta^{18}O_{shell}$ patterns in which $\delta^{18}O_{water}$ values reach a maximum during colder temperatures, supporting this interpretation.

Estimated LGM snowfall

Using a linear mixing model, the proportion of snowmelt contribution to the springs that fed paleo-Lake Hula during the LGM can be estimated. During the LGM, $\delta^{18}O_{water}$ values in precipitation were approximately 2.5‰ higher than present (Bar-Matthews et al., 2003), and modern monthly $\delta^{18}O_{water}$ values in Mt. Hermon precipitation range from approximately −10.5 to −5.0‰ (Ayalon et al., 2013) and serve as the modern endmember $\delta^{18}O_{water}$ values for snow and rain recharge to the springs, respectively. Thus, the equivalent $\delta^{18}O_{water}$ values of precipitation during the LGM are considered to be −8.0‰ and −2.5‰ for snow and rain, respectively. For a lake with a short residence time of less than 6 months, the highest and lowest values of the modeled $\delta^{18}O_{water}$ values are expected to reflect the endmembers of local precipitation (winter) and spring water (summer), respectively. Based on the model LGM shell, the summer $\delta^{18}O_{water}$ endmember (−7.1‰) is composed of 84% snowmelt. This is much greater than the modern values of 30% (Gil'ad and Bonne, 1990) and the estimate of at least 40% contribution of snow during the LGM by Zaarur et al. (2016).

However, these calculations are subject to considerable uncertainty. The model of $\delta^{18}O_{water}$ relies on the modeled temperature during shell formation. Changing the temperature would result in a change in modeled $\delta^{18}O_{water}$ of ~0.24‰/°C. For lower lake temperatures, this would lead to a lower estimate of snow recharge of ~5%/°C. Clumped isotope-based temperatures from nearby LGM *Melanopsis* specimens fall in a range similar to modern shells or up to 3°C colder (Zaarur et al., 2016). This is in line with our model, which estimates an average lake temperature of ~16°C during the LGM, about 2°C colder than the modern Jordan River. However, clumped isotope evidence from Soreq Cave suggests an ~10−12°C temperature change in the same time interval (Affek et al., 2008; Matthews et al., 2021). Although the snail-shell temperatures more closely reflect summer-growth temperatures, lake temperatures 10°C colder than modern are unlikely, as this would be colder than modern *Melanopsis* habitats. The discrepancy could be due in part to temperature buffering in the lake, where water temperatures, especially in cold regions, are warmer than the mean annual temperatures (Hren and Sheldon, 2012). For an air temperature of 11°C (~10°C colder than modern), annual average lake temperatures are estimated to be 14.8°C according to the transfer function given by Hren and Sheldon (2012), which would result in a snow-recharge estimate of ~78%. Alternatively, the effect of lower ground temperatures in the mountains could result in snow with lower $\delta^{18}O$ values, resulting in an overestimate of the spring-water contribution from snow. Lower sea levels also lead to increased effective altitude, which could also lower $\delta^{18}O_{snow}$ values. On the other hand, evaporation of inflowing water before it reaches the snail's habitat would result in higher $\delta^{18}O_{water}$ values compared with spring discharge, which ultimately results in an underestimate of snow recharge. In addition, if the lake has a longer residence time, which is likely given the larger inferred lake size, then the buffering effect of lake water mixing with the input from local precipitation and spring water would also need to be taken into account.

Archaeological implications

The results presented here are based upon a small sample. Nevertheless, when compared with pollen and archaeological sequences, they demonstrate the great potential of isotopic sclerochronological studies for high-resolution, seasonal reconstruction

of the paleoenvironment and its impact on human presence and activity in the region. The origin of the shells from a long, well-dated sequence and defined cultural scheme, combined with subsampling of each shell, makes sclerochronological analysis a powerful tool for comparison and calibration of the different environmental proxies present at JRD. Importantly, the evidence for more snow during the glacial conditions in the Hula Valley can explain the dry signal obtained for this interval from the JRD pollen diagrams (Langgut et al., 2021). Although this signal is normally interpreted as indicating dry conditions, cold climatic conditions with more snow may result in less arboreal pollen.

The JRD archaeological sequence documents 10,000 years of human activity on the shore of paleo-Lake Hula. During this time, the region witnessed the dramatic cultural and economic transition from small bands of nomadic hunter- (and fisher) gatherers to the early sedentary settlements of the Natufian to the agricultural communities of the Neolithic era. The results presented here contribute to a better understanding of the environmental background for these cultural and economic changes. The evidence for warmer and wetter conditions in Layer 3C correlates well with the results of other environmental proxies from JRD (Sharon et al., 2020; Langgut et al., 2021), which mark changing conditions at the onset of the Natufian. Interrelations between human cultural changes and paleoenvironment changes are highly complex and debatable; hence, reliable environmental reconstruction is a highly significant foundation for any such discussion.

CONCLUSIONS

Late Pleistocene and modern *Melanopsis* shells from the Hula Basin were sampled to produce $\delta^{18}O$ and $\delta^{13}C$ data with sub-monthly resolution. However, growth marks present in the shells indicate that shell growth slows or stops during winter, inhibiting a full assessment of seasonality.

Applying the results of the modern shell to subfossil isotope data from JRD yielded valuable information about seasonality and the environment of the Hula Basin. Shells from layers dated to the LGM exhibited small fluctuations in $\delta^{18}O_{shell}$ and $\delta^{13}C_{shell}$ values, indicating a large, buffered waterbody. The lack of strong correlation between $\delta^{18}O_{shell}$ and $\delta^{13}C_{shell}$ values indicates that the paleolake was hydrologically open with a relatively short residence time. The data support an increased water contribution from the Hula Valley during the Lake Lisan high stand. Furthermore, relatively high $\delta^{18}O_{shell}$ values immediately after growth marks and a subsequent trend toward lower values may indicate that local precipitation had higher $\delta^{18}O_{water}$ values than spring waters. This observation supports a greater proportion of snowmelt contribution in regional groundwater recharge during this time interval, perhaps more than double the amount of present-day snowmelt.

In contrast, data from shells that likely formed during the drier conditions of Heinrich 1 indicate a significantly smaller waterbody, and data from Bølling-Allerød shells point to an intermediate-sized waterbody. Fluctuations in waterbody size at JRD qualitatively agree with changes in lake level of Lake Lisan, supporting the Hula Valley as a major contributor to changes in water balance in the catchment.

These results agree well with palynological results from JRD (Langgut et al., 2021) and provide additional context for understanding other environmental proxies collected at the site. Furthermore, these data give insight into weather-scale events and seasonality during the final part of the late Pleistocene in the Levant.

REFERENCES

Affek, H.P., Bar-Matthews, M., Ayalon, A., Matthews, A., Eiler, J.M., 2008. Glacial/interglacial temperature variations in Soreq cave speleothems as recorded by "clumped isotope" thermometry. *Geochimica et Cosmochimica Acta* **72**, 5351–5360.

Aharonovich, S., Sharon, G., Weinstein-Evron, M., 2014. Palynological investigations at the Middle Palaeolithic site of Nahal Mahanayeem Outlet, Israel. *Quaternary International* **331**, 149–166.

Ayalon, A., Bar-Matthews, M., Frumkin, A., Matthews, A., 2013. Last Glacial warm events on Mount Hermon: the southern extension of the Alpine karst range of the east Mediterranean. *Quaternary Science Reviews* **59**, 43–56.

Babad, A., Burg, A., Adar, E.M., 2020. Conceptual hydrological approach to a geologically complex basin with scarce data: the Hula Valley, Middle East. *Hydrogeology Journal* **28**, 703–722.

Bar-Matthews, M., Ayalon, A., Gilmour, M., Matthews, A., Hawkesworth, C.J., 2003. Sea–land oxygen isotopic relationships from planktonic foraminifera and speleothems in the Eastern Mediterranean region and their implication for paleorainfall during interglacial intervals. *Geochimica et Cosmochimica Acta* **67**, 3181–3199.

Bar-Matthews, M., Ayalon, A., Kaufman, A., Wasserburg, G.J., 1999. The Eastern Mediterranean paleoclimate as a reflection of regional events: Soreq cave, Israel. *Earth and Planetary Science Letters* **166**, 85–95.

Bar-Matthews, M., Keinan, J., Ayalon, A., 2019. Hydro-climate research of the late Quaternary of the Eastern Mediterranean-Levant region based on speleothems research—a review. *Quaternary Science Reviews* **221**, 105872.

Bartolini, F., Aquiloni, L., Nisi, B., Nuccio, C., Vaselli, O., Cianfanelli, S., 2017. Divergent demographic patterns and perspectives for conservation of endemic species in extreme environments: a case study of the springsnail *Melanopsis etrusca* (Gastropoda: Melanopsidae). *Invertebrate Biology* **136**, 441–455.

Bartov, Y., Goldstein, S.L., Stein, M., Enzel, Y., 2003. Catastrophic arid episodes in the Eastern Mediterranean linked with the North Atlantic Heinrich events. *Geology* **31**, 439–442.

Bartov, Y., Stein, M., Enzel, Y., Agnon, A., Reches, Z., 2002. Lake levels and sequence stratigraphy of Lake Lisan, the Late Pleistocene precursor of the Dead Sea. *Quaternary Research* **57**, 9–21.

Belfer-Cohen, A., Goring-Morris, N., 2020. From the Epipalaeolithic into the earliest Neolithic (PPNA) in the South Levant. *Documenta Praehistorica* **47**, 36–52.

Belfer-Cohen, A., Goring-Morris, N., 2013. Breaking the mold: phases and facies in the Natufian of the Mediterranean zone. In: Bar-Yosef, O., Valla, F.R. (Eds.), *Natufian Foragers in the Levant: Terminal Pleistocene Social Changes in Western Asia*. International Monographs in Prehistory, Ann Arbor, MI, pp. 543–561.

Ben Dor, Y., Armon, M., Ahlborn, M., Morin, E., Erel, Y., Brauer, A., Schwab, M.J., Tjallingii, R., Enzel, Y., 2018. Changing flood frequencies under opposing late Pleistocene eastern Mediterranean climates. *Scientific Reports* **8**, 8445.

Ben Dor, Y., Marra, F., Armon, M., Enzel, Y., Morin, E., 2021. Hydroclimatic variability of opposing late Pleistocene climates in the

Levant revealed by deep Dead Sea sediments. *Climate of the Past Discussions*, 1–31.

Develle, A.L., Gasse, F., Vidal, L., Williamson, D., Demory, F., Van Campo, E., Ghaleb, B., Thouveny, N., 2011. A 250ka sedimentary record from a small karstic lake in the Northern Levant (Yammoûneh, Lebanon). Paleoclimatic implications. *Palaeogeography, Palaeoclimatology, Palaeoecology* 305, 10–27.

Dimentman, C., Bromley, H.J., Por, F.D., 1992. *Lake Hula: Reconstruction of the Fauna and Hydrobiology of a Lost Lake*. Jerusalem: Israel Academy of Sciences and Humanities.

Elkarmi, A.Z., Ismail, N.S., 2006. Allometry of the gastropod *Melanopsis praemorsa* (Thiaridae: Prosobranchia) from Azraq Oasis, Jordan. *Pakistan Journal of Biological Sciences* 9, 1359–1363.

Enzel, Y., Amit, R., Dayan, U., Crouvi, O., Kahana, R., Ziv, B., Sharon, D., 2008. The climatic and physiographic controls of the eastern Mediterranean over the late Pleistocene climates in the southern Levant and its neighboring deserts. *Global and Planetary Change* 60, 165–192.

Enzel, Y., Bar-Yosef, O. (Eds.), 2017. *Quaternary of the Levant: Environments, Climate Change, and Humans*. Cambridge: Cambridge University Press.

Falniowski, A., Heller, J., Cameron, R.A.D., Pokryszko, B.M., Osikowski, A., Rysiewska, A., Hofman, S., 2020. Melanopsidae (Caenogastropoda: Cerithioidea) from the eastern Mediterranean: another case of morphostatic speciation. *Zoological Journal of the Linnean Society* 190, 483–507.

Frumkin, A., Bar-Yosef, O., Schwarcz, H.P., 2011. Possible paleohydrologic and paleoclimatic effects on hominin migration and occupation of the Levantine Middle Paleolithic. *Journal of Human Evolution* 60, 437–451.

Gat, J.R., 1970. Environmental isotope balance of Lake Tiberias. In: *Isotope Hydrology: Proceedings of a Symposium on Use of Isotopes in Hydrology*. Vienna: International Atomic Energy Agency, pp. 109–127.

Gat, J.R., Dansgaard, W., 1972. Stable isotope survey of the fresh water occurrences in Israel and the Northern Jordan Rift Valley. *Journal of Hydrology* 16, 177–211.

Geary, D.H., Hoffmann, E., Magyar, I., Freiheit, J., Padilla, D., 2012. Body size, longevity, and growth rate in Lake Pannon melanopsid gastropods and their predecessors. *Paleobiology* 38, 554–568.

Gil'ad, D., Bonne, J., 1990. The snowmelt of Mt. Hermon and its contribution to the sources of the Jordan River. *Journal of Hydrology* 114, 1–15.

Glaubrecht, M., 1993. Mapping the diversity: geographical distribution of the freshwater snail *Melanopsis* (Gastropoda:? Cerithioidea: Melanopsidae) with focus on its systematics in the Mediterranean basin. *Mitteilungen aus dem Hamburgischen Zoologischen Museum und Institut* 90, 41–97.

Gophen, M., Meron, M., Tsipris, Y., Orlov-Levin, V., Peres, M., 2016. Chemical, hydrological and climatological properties of Lake Agmon, Hula Valley (Israel), (1994–2006). *Open Journal of Modern Hydrology* 6, 8–18.

Gophen, M., Tsipris, Y., Meron, M., Bar-Ilan, I., 2003. The management of Lake Agmon wetlands (Hula Valley, Israel). *Hydrobiologia* 506–509, 803–809.

Goren-Inbar, N., Sharon, G., Melamed, Y., Kislev, M., 2002a. Nuts, nut cracking, and pitted stones at Gesher Benot Ya'aqov, Israel. *Proceedings of the National Academy of Sciences USA* 99, 2455–2460.

Goren-Inbar, N., Werker, E., Feibel, C.S., 2002b. *The Acheulian Site of Gesher Benot Ya'aqov, Israel: The Wood Assemblage*. Oxford: Oxbow Books.

Goring-Morris, N., Belfer-Cohen, A., 2017. The Early and Middle Epipalaeolithic of Cisjordan. In: Enzel, Y., Bar-Yosef, O. (Eds.), *Quaternary of the Levant: Environments, Climate Change, and Humans*. Cambridge: Cambridge University Press, pp. 639–650.

Hartman, G., Bar-Yosef, O., Brittingham, A., Grosman, L., Munro, N.D., 2016. Hunted gazelles evidence cooling, but not drying, during the Younger Dryas in the southern Levant. *Proceedings of the National Academy of Sciences USA* 113, 3997–4002.

Hazan, N., Stein, M., Agnon, A., Marco, S., Nadel, D., Negendank, J.F.W., Schwab, M.J., Neev, D., 2005. The late Quaternary limnological history of Lake Kinneret (Sea of Galilee), Israel. *Quaternary Research* 63, 60–77.

Heimann, A., Zilberman, E., Amit, R., Frieslander, U., 2009. Northward migration of the southern diagonal fault of the Hula pull-apart basin, Dead Sea transform, northern Israel. *Tectonophysics* 476, 496–511.

Heller, J., Mordan, P., Ben-Ami, F., Sivan, N., 2005. Conchometrics, systematics and distribution of *Melanopsis* (Mollusca: Gastropoda) in the Levant. *Zoological Journal of the Linnean Society* 144, 229–260.

Horowitz, A., 1973. Development of the Hula Basin, Israel. *Israel Journal of Earth Sciences* 22, 107–139.

Hren, M.T., Sheldon, N.D., 2012. Temporal variations in lake water temperature: paleoenvironmental implications of lake carbonate $\delta^{18}O$ and temperature records. *Earth and Planetary Science Letters* 337–338, 77–84.

Iljina, L.B., Frolov, P.D., 2010. Shell morphology and microstructure of Neogene *Melanopsis* Ferussac (Gastropoda). *Paleontological Journal* 44, 489–493.

Israel Meteorological Service, 2018. Weather Records, Kfar Blum and Dafna. https://ims.gov.il/en/data_gov.

Keinan, J., Bar-Matthews, M., Ayalon, A., Zilberman, T., Agnon, A., Frumkin, A., 2019. Paleoclimatology of the Levant from Zalmon Cave speleothems, the northern Jordan Valley, Israel. *Quaternary Science Reviews* 220, 142–153.

Kim, S.T., Mucci, A., Taylor, B.E., 2007a. Phosphoric acid fractionation factors for calcite and aragonite between 25 and 75 °C: Revisited. *Chemical Geology* 246, 135–146.

Kim, S.T., O'Neil, J.R., Hillaire-Marcel, C., Mucci, A., 2007b. Oxygen isotope fractionation between synthetic aragonite and water: influence of temperature and Mg^{2+} concentration. *Geochimica et Cosmochimica Acta* 71, 4704–4715.

Langgut, D., Cheddadi, R., Sharon, G., 2021. Climate and environmental reconstruction of the Epipaleolithic Mediterranean Levant (22.0–11.9 ka cal. BP). *Quaternary Science Reviews* 270, 107170.

Leng, M.J., Marshall, J.D., 2004. Palaeoclimate interpretation of stable isotope data from lake sediment archives. *Quaternary Science Reviews* 23, 811–831.

Lev, L., Stein, M., Ito, E., Fruchter, N., Ben-Avraham, Z., Almogi-Labin, A., 2019. Sedimentary, geochemical and hydrological history of Lake Kinneret during the past 28,000 years. *Quaternary Science Reviews* 209, 114–128.

Litaor, M.I., Eshel, G., Sade, R., Rimmer, A., Shenker, M., 2008. Hydrogeological characterization of an altered wetland. *Journal of Hydrology* 349, 333–349.

Ludwig, P., Hochman, A., 2022. Last glacial maximum hydro-climate and cyclone characteristics in the Levant: a regional modelling perspective. *Environmental Research Letters* 17, 014053.

Mannino, M.A., Thomas, K.D., Leng, M.J., Sloane, H.J., 2008. Shell growth and oxygen isotopes in the topshell *Osilinus turbinatus*: resolving past inshore sea surface temperatures. *Geo-Marine Letters* 28, 309–325.

Marder, O., Biton, R., Boaretto, E., Feibel, C., Melamed, Y., Mienis, H. K., Rabinovich, R., Zohar, I., Sharon, G., 2015. Jordan River Dureijat—a new Epipaleolithic site in the Upper Jordan Valley. *Journal of the Israel Prehistoric Society*, 45, 5–30.

Matthews, A., Affek, H.P., Ayalon, A., Vonhof, H.B., Bar-Matthews, M., 2021. Eastern Mediterranean climate change deduced from the Soreq Cave fluid inclusion stable isotopes and carbonate clumped isotopes record of the last 160 ka. *Quaternary Science Reviews* 272, 107223.

Melamed, Y., Kislev, M.E., Geffen, E., Lev-Yadun, S., Goren-Inbar, N., 2016. The plant component of an Acheulian diet at Gesher Benot Ya'aqov, Israel. *Proceedings of the National Academy of Sciences USA* 113, 14674–14679.

Miebach, A., Chen, C., Schwab, M.J., Stein, M., Litt, T., 2017. Vegetation and climate during the Last Glacial high stand (ca. 28–22 ka BP) of the Sea of Galilee, northern Israel. *Quaternary Science Reviews* 156, 47–56.

Miebach, A., Stolzenberger, S., Wacker, L., Hense, A., Litt, T., 2019. A new Dead Sea pollen record reveals the last glacial paleoenvironment of the southern Levant. *Quaternary Science Reviews* 214, 98–116.

Moulin, A., Benedetti, L., Vidal, L., Hage-hassan, J., Elias, A., Woerd, J. Van Der, Tapponnier, P., Schimmelpfennig, I., Da, M., 2022. LGM glaciers in the SE Mediterranean? First evidence from glacial landforms and ^{36}Cl dating on Mount Lebanon. *Quaternary Science Reviews* 285.

Müller, D., Neugebauer, I., Dor, Y. Ben, Enzel, Y., Schwab, M.J., 2022. Phases of stability during major hydroclimate change ending the Last Glacial in the Levant. *Scientific Reports* 12, 6052.

Orland, I.J., Bar-Matthews, M., Ayalon, A., Matthews, A., Kozdon, R., Ushikubo, T., Valley, J.W., 2012. Seasonal resolution of Eastern Mediterranean climate change since 34 ka from a Soreq Cave speleothem. *Geochimica et Cosmochimica Acta* 89, 240–255.

Rambeau, C.M.C., 2010. Palaeoenvironmental reconstruction in the Southern Levant: synthesis, challenges, recent developments and perspectives. *Philosophical Transactions of the Royal Society A: Mathematical, Physical and Engineering Sciences* **368**, 5225–5248.

Rice, A., 2018. Stable Isotope Sclerochronology of *Melanopsis* (Gastropoda) Shells: Inferring Late Pleistocene Seasonality in the Upper Jordan River Valley. MSc thesis. University of Iceland, Reykjavík.

Rimmer, A., Salingar, Y., 2006. Modelling precipitation-streamflow processes in karst basin: the case of the Jordan River sources, Israel. *Journal of Hydrology* **331**, 524–542.

Rindsberger, M., Jaffe, Sh., Rahamim, Sh., Gat, J.R., 1990. Patterns of the isotopic composition of precipitation in time and space: data from the Israeli storm water collection program. *Tellus* **42B**, 263–271.

Roberts, N., Jones, M.D., Benkaddour, A., Eastwood, W.J., Filippi, M.L., Frogley, M.R., Lamb, H.F., *et al.*, 2008. Stable isotope records of Late Quaternary climate and hydrology from Mediterranean lakes: the ISOMED synthesis. *Quaternary Science Reviews* **27**, 2426–2441.

Robinson, S.A., Black, S., Sellwood, B.W., Valdes, P.J., 2006. A review of palaeoclimates and palaeoenvironments in the Levant and Eastern Mediterranean from 25,000 to 5000 years BP: setting the environmental background for the evolution of human civilisation. *Quaternary Science Reviews* **25**, 1517–1541.

Rossignol-Strick, M., 1995. Sea-land correlation of pollen records in the Eastern Mediterranean for the glacial-interglacial transition: biostratigraphy versus radiometric time-scale. *Quaternary Science Reviews* **14**, 893–915.

Rybakov, M., Fleischer, L., ten Brink, U., 2003. The Hula Valley subsurface structure inferred from gravity data. *Israel Journal of Earth Sciences* **52**, 113–122.

Saaroni, H., Ziv, B., 2000. Summer rain episodes in a Mediterranean climate, the case of Israel: climatological–dynamical analysis. *International Journal of Climatology* **20**, 191–209.

Sade, R., Rimmer, A., Samuels, R., Salingar, Y., Denisyuk, M., Alpert, P., 2016. Water management in a complex hydrological basin—application of Water Evaluation and Planning Tool (WEAP) to the Lake Kinneret watershed, Israel. In: Borchardt, D., Bogardi, J., Ibisch, R. (Eds.), *Integrated Water Resources Management: Concept, Research and Implementation*. Cham, Switzerland: Springer International, pp. 35–57.

Schattner, U., Weinberger, R., 2008. A mid-Pleistocene deformation transition in the Hula basin, northern Israel: implications for the tectonic evolution of the Dead Sea Fault. *Geochemistry, Geophysics, Geosystems* **9**.

Schmitz, B., Andreasson, F.P., 2001. Air humidity and lake δ^{18}O during the latest Paleocene – earliest Eocene in France from recent and fossil freshwater and marine gastropod δ^{18}O, δ^{13}C, and ^{87}Sr/^{86}Sr. *Geological Society of America Bulletin* **113**, 774–789.

Schöne, B.R., Rodland, D.L., Wehrmann, A., Heidel, B., Oschmann, W., Zhang, Z., Fiebig, J., Beck, L., 2007. Combined sclerochronologic and oxygen isotope analysis of gastropod shells (*Gibbula cineraria*, North Sea): life-history traits and utility as a high-resolution environmental archive for kelp forests. *Marine Biology* **150**, 1237–1252.

Sharon, G., Grosman, L., Allué, E., Barash, A., Bar-Yosef Mayer, D.E., Biton, R., Bunin, E.J., *et al.*, 2020. Jordan River Dureijat: 10,000 years of intermittent Epipaleolithic activity on the shore of Paleolake Hula. *PaleoAnthropology* **34**, 64.

Spiro, B., Ashkenazi, S., Mienis, H.K., Melamed, Y., Feibel, C., Delgado, A., Starinsky, A., 2009. Climate variability in the Upper Jordan Valley around 0.78 Ma, inferences from time-series stable isotopes of Viviparidae, supported by mollusc and plant palaeoecology. *Palaeogeography, Palaeoclimatology, Palaeoecology* **282**, 32–44.

Spiro, B., Ashkenazi, S., Starinsky, A., Katz, A., 2011. Strontium isotopes in *Melanopsis* sp. as indicators of variation in hydrology and climate in the Upper Jordan Valley during the Early-Middle Pleistocene, and wider implications. *Journal of Human Evolution* **60**, 407–416.

Stockhecke, M., Timmermann, A., Kipfer, R., Haug, G.H., Kwiecien, O., Friedrich, T., Menviel, L., Litt, T., Pickarski, N., Anselmetti, F.S., 2016. Millennial to orbital-scale variations of drought intensity in the Eastern Mediterranean. *Quaternary Science Reviews* **133**, 77–95.

Taft, L., Mischke, S., Wiechert, U., Leipe, C., Rajabov, I., Riedel, F., 2014. Sclerochronological oxygen and carbon isotope ratios in *Radix* (Gastropoda) shells indicate changes of glacial meltwater flux and temperature since 4,200 cal yr BP at Lake Karakul, eastern Pamirs (Tajikistan). *Journal of Paleolimnology* **52**, 27–41.

Taft, L., Wiechert, U., Albrecht, C., Leipe, C., Tsukamoto, S., Wilke, T., Zhang, H., Riedel, F., 2020. Intra-seasonal hydrological processes on the western Tibetan Plateau: monsoonal and convective rainfall events at ~7.5 ka. *Quaternary International* **537**, 9–23.

Tchernov, E., 1973. *On the Pleistocene Molluscs of the Jordan River Valley*. Jerusalem: Israel Academy of Sciences and Humanities.

Torfstein, A., Goldstein, S.L., Stein, M., Enzel, Y., 2013. Impacts of abrupt climate changes in the Levant from Last Glacial Dead Sea levels. *Quaternary Science Reviews* **69**, 1–7.

Vaks, A., Bar-Matthews, M., Ayalon, A., Matthews, A., Frumkin, A., Dayan, U., Halicz, L., Almogi-Labin, A., Schilman, B., 2006. Paleoclimate and location of the border between Mediterranean climate region and the Saharo-Arabian Desert as revealed by speleothems from the northern Negev Desert, Israel. *Earth and Planetary Science Letters* **249**, 384–399.

Wiese, R., Hartmann, K., Gummersbach, V.S., Shemang, E.M., Struck, U., Riedel, F., 2020. Lake highstands in the northern Kalahari, Botswana, during MIS 3b and LGM. *Quaternary International* **558**, 10–18.

Winter, N.J. de, 2022. ShellChron 0.4.0: a new tool for constructing chronologies in accretionary carbonate archives from stable oxygen isotope profiles. *Geoscientific Model Development* **15**, 1247–1267.

Zaarur, S., Affek, H.P., Stein, M., 2016. Last glacial-Holocene temperatures and hydrology of the Sea of Galilee and Hula Valley from clumped isotopes in *Melanopsis* shells. *Geochimica et Cosmochimica Acta* **179**, 142–155.

Zeist, W. van, Baruch, U., Bottema, S., 2009. Holocene palaeoecology of the Hula area, northeastern Israel. In: Kaptijn, E., Petit, L.P. (Eds.), *A Timeless Vale*. Archeological Studies Leiden University 19. Leiden: Leiden University Press, pp. 29–64.